AXAF COATING PROCESS SELECTION STUDY: REFLECTIVITY MEASUREMENTS

Prepared by: Patrick Slane

3 November 1992

Contents

List of Figures

List of Tables

1 Introduction

In an effort to maximize the x-ray throughput of the AXAF-I HRMA, extensive studies of x-ray reflectivity have been carried out at SAO, in conjunction with personnel at MSFC and TRW (Slane 1990a). These studies have included both theoretical and experimental investigations of a number of factors affecting x-ray reflectivity. Results of initial studies, which we summarize below, led to the conclusion that the original baseline HRMA, which had gold (Au) coatings for the 3 inner mirrors and nickel (Ni) coatings for the outer mirrors, would have increased effective area by substituting iridium (Ir) for gold. Further, the studies suggested that the nature of the deposition process could strongly affect the resulting x-ray performance of the coatings, and that further study of available processes could lead to an enhanced mirror throughput. The AXAF Coating Process Selection Study (CPSS) was conceived to address these issues by formulating a matrix of test elements that would lead to a final recommendation for the baseline HRMA coating. The elements of the plan were arrived at in a meeting of the Coating Working Group, at MSFC in December 1991 (Loer and Hixson 1991). Herein we present the results of this study which have led the Coating Working Group to recommend iridium as the baseline coating for the AXAF-I mission, and have allowed the specification of a minimum performance criterion for the coatings, based upon laboratory measurements of coated samples.

1.1 X-ray Reflectivity at AXAF Energies

From an astrophysics point of view, a significant feature of AXAF is the high energy response; in contrast to the *Einstein* and ROSAT observatories which extended only to $\sim$ 4 keV and $\sim$ 2 keV, respectively, the AXAF effective area extends to 10 keV. This will allow new spectroscopic investigations to be carried out, including studies of thermal spectra at temperatures typical of clusters of galaxies as well as investigations in the astrophysically important Fe-line region. These goals require an effective area which remains large at higher energies, and this in turn places constraints on the mirror coatings; only through careful selection of coating materials and methods will the reflectivity of the coatings be sufficient to meet the goals of the mirror design.

One primary concern with regard to thin film coatings centers on the effective density ρ of the coating material. Because thin films tend to grow in discrete "islands" which eventually coalesce, there may be considerable open space in the resulting coating. As discussed below (Section 1.1.1), the optical behavior of the coatings may be characterized by a complex dielectric constant κ. At x-ray energies, total external reflection occurs at a critical angle

$$\theta_c \approx \sqrt{\alpha} \tag{1}$$

where $1-\alpha$ is the real part of the dielectric constant. Because $\alpha \propto \rho$ (see below), we see that the critical angle θ_c scales as $\rho^{1/2}$. Thus, identification of the critical angle through measurements of reflectivity as a function of grazing angle provides a relatively sensitive indicator of the coating density. This is illustrated in Figure 1 which contains a plot of reflectivity vs grazing angle, for 8.03 keV x-rays, for an ideal iridium coating as well as one with 80% bulk density. Figure 2 illustrates the behavior of the x-ray reflectivity as a function of energy (for a grazing angle of 30 arcmin) for an ideal coating and for a coating with iridium density equal to 80% that of the bulk material.

It is clear that the effects of reduced density are most pronounced at higher energies; as a result, we have carried out measurements at 8.03 keV for the Au, Pt, and Ir coatings. For Ni coatings we have carried out measurements at 6.4 keV, which provides a good probe of the critical angle region for this material.

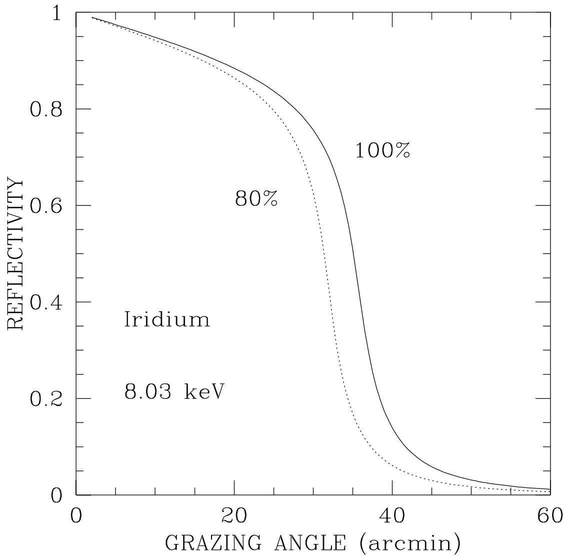

Figure 1: *X-ray reflectivity as a function of grazing angle for iridium coatings with 100% (solid) and 80% bulk density. X-ray energy is 8.03 keV.*

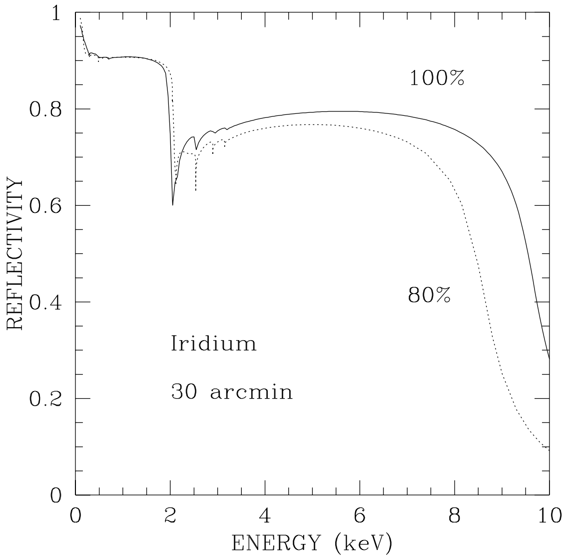

Figure 2: *X-ray reflectivity as a function of energy for iridium coatings with 100% (solid) and 80% bulk density. Grazing angle is 30 arcmin.*

1.1.1 Fundamentals of grazing incidence reflectivity: a summary

Optical Constants

In order to calculate the theoretical reflectivity for a given coating, it is necessary to know the optical constants associated with the coating material. A list of such constants, and a review of reflectivity calculations, is given in Zombeck (1983a). Elsner *et al.* (1991) have presented a review and critical assessment of the standard approach to deriving optical constants for use in x-ray reflectivity calculations. Summarizing their description, following that of Henke (1982), the optical constants are most conveniently expressed in the form of a complex dielectric constant:

$$\kappa = 1 - \alpha - i\gamma. \tag{2}$$

The real and imaginary parts of the dielectric constant are associated with the atomic scattering factors f_1 and f_2 (which are derived from the photoabsorption coefficient $\mu_a(E)$):

$$\alpha = \frac{1}{\pi}\left(\frac{e^2}{m_e c^2}\right)\left(\frac{N_0\rho}{A}\right)\left(\frac{hc}{E}\right)^2 f_1,$$

and

$$\gamma = \frac{1}{\pi}\left(\frac{e^2}{m_e c^2}\right)\left(\frac{N_0\rho}{A}\right)\left(\frac{hc}{E}\right)^2 f_2. \tag{3}$$

Here m_e is the electron mass, N_0 is Avagadro's number, ρ is the density, A is the atomic weight, and other fundamental constants are expressed with standard symbols.

Often, the optical constants are expressed in terms of a complex refractive index:

$$\tilde{n} = 1 - \delta - i\beta. \tag{4}$$

Since

$$\tilde{n} = \kappa^{1/2}, \tag{5}$$

δ and β may be derived directly from α and γ:

$$\delta = 1 - \sqrt{\frac{1}{2}\left[\sqrt{(1-\alpha)^2 + \gamma^2} + (1-\alpha)\right]}, \tag{6}$$

$$\beta = \mathrm{sgn}(\gamma)\sqrt{\frac{1}{2}\left[\sqrt{(1-\alpha)^2 + \gamma^2} - (1-\alpha)\right]}. \tag{7}$$

Fresnel Equations

Given the optical constants of the coating material, the reflectivity may be calculated as a function of energy and grazing angle by using the Fresnel equations:

$$R_{\perp} = \frac{a^2 + b^2 - 2a\cos\theta + \cos^2\theta}{a^2 + b^2 + 2a\cos\theta + \cos^2\theta} \tag{8}$$

and

$$R_{\parallel} = \frac{a^2 + b^2 - 2a\sin\theta\tan\theta + \sin^2\theta\tan^2\theta}{a^2 + b^2 + 2a\sin\theta\tan\theta + \sin^2\theta\tan^2\theta} \tag{9}$$

where

$$\begin{aligned} 2a^2 &= \left[\left(n^2 - \beta^2 - \sin^2\theta\right)^2 + 4n^2\beta^2\right]^{1/2} \\ &\quad + \left(n^2 + \beta^2 - \sin^2\theta\right), \end{aligned} \tag{10}$$

and

$$\begin{aligned} 2b^2 &= \left[\left(n^2 - \beta^2 - \sin^2\theta\right)^2 + 4n^2\beta^2\right]^{1/2} \\ &\quad - \left(n^2 + \beta^2 - \sin^2\theta\right). \end{aligned} \tag{11}$$

Here θ is the angle of incidence (*i.e.* $\pi/2$ - grazing angle) and $n = 1 - \delta$. A comparison of the various sets of constants has been carried out by Elsner (1991), who has recommended the use of constants compiled by Henke *et al.* (1991) for AXAF-related calculations; such a convention has been adopted for the remainder of this report.

1.1.2 Deposition techniques: methods and considerations

One factor which may play a considerable role in determining the density profile of a deposited thin film is the mobility of the atoms as they deposit on the substrate; higher mobility promotes formation of more nucleation sites and, thus, a closer-packed structure. High mobility may be achieved by ensuring that the atoms being deposited are reasonably energetic upon arrival at the substrate. This, in turn, is accomplished by providing energetic atoms at the site of the target, and by using low ambient pressure to minimize collisional energy losses as the atoms migrate from target to substrate. While evaporative processes are generally carried out at pressures below 10^{-5} torr, the energy of the atoms as they leave the target material is relatively low. Thus, the mobility upon arrival at the substrate is not sufficient to prevent formation of columnar growth associated with the development of voids. In some modes of operation an ion beam is used to assist the deposition process by supplying additional energy to the atoms via bombardment with accelerated ions.

Sputtering processes, on the other hand, provide considerable energy to the target atoms via bombardment with energetic ions of a noble gas. Ambient pressures, however, tend to be higher because of the presence of the sputtering gas. Minimization of the sputter-gas pressure, as well as of the target-substrate distance, is necessary to achieve more densely packed coatings.

1.1.3 Materials

Reflective coatings for previous x-ray missions have included a number of different materials: Ni for *Einstein*, Au for ROSAT and BBXRT, and Ir for SAX to name a few. For the range of grazing angles appropriate for AXAF, Ni cannot provide high energy response; as a result, the baseline coating for the AXAF-I mirrors originally included Au for the innermost mirrors (Zombeck 1983b). While Au reflects well at the lower energies as well, there are absorption features that reduce the reflectivity in the vicinity of 2.2 keV. To compensate for this loss, the baseline plan was to coat the outermost mirrors with Ni, which would introduce absorption edges at 0.8 keV, but partially fill in the Au edges.

While the choice of Au to provide high energy response has a secure basis (it has been used successfully on previous missions, and considerable expertise in producing Au coatings exists in the coating industry), platinum (Pt) and Ir

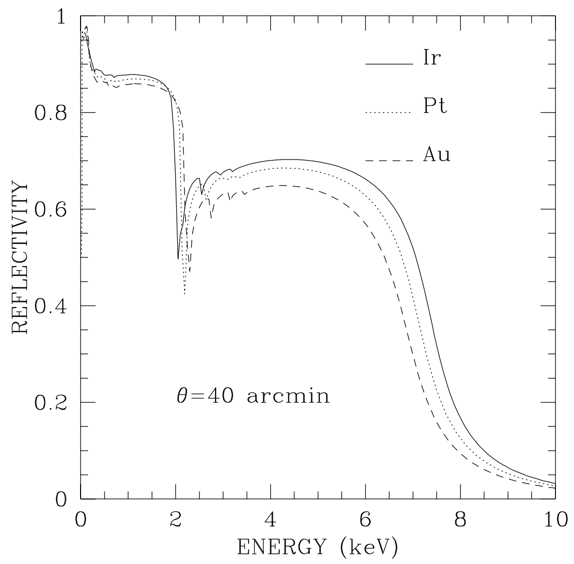

Figure 3: *X-ray reflectivity vs energy for Ir, Pt, and Au at a grazing angle of 40 arcmin.*

coatings offer the potential for even better high energy performance. The theoretical reflectivity for these materials is plotted as a function of energy, for a grazing angle of 40 arcmin, in Figure 3. Experience has shown, however, that one often obtains less than the theoretically predicted reflectivity on actual samples. To determine whether a change from Au to another material would be beneficial, coatings of Pt and Ir were produced using both evaporative and sputtering techniques.

1.1.4 Previous AXAF reflectivity study results

Studies of x-ray reflectivity measurements carried out at SAO prior to the CPSS were summarized by Slane *et al.* (1991). The studies involved measurements of more than 75 mirrors, testing such parameters as coating material, deposition process, deposition angle, and coating thickness. Measurements were carried out primarily at 8.03 and 6.4 keV, with some additional measurements at 4.5 and 1.5 keV. Several distinct conclusions were reached from these studies:

1. X-ray reflectivity may be strongly affected by coating thickness; the thinner coatings ($\sim$ 200 Å) performed better than the thicker coatings ($\sim$ 750 Å). This difference was particularly significant for samples produced by evaporative methods, and is likely to be related to changes in film morphology as thickness increases.

2. The effective density of the films increases with depth into the coating. This is evident from measurements at different energies; measurements made at 8.03 keV suggest a coating with higher density than measurements made at 6.4 keV (Slane 1990b). The interpretation is that the lower energy measurements sample only the upper portions of the coating, which apparently are somewhat "fluffy" with low effective density (*e.g.* 80% that of the bulk material), while higher energy measurements sample deeper into the coating where the film growth has permitted fewer voids between the crystalline islands.

3. Deposition should be carried out at near-normal incidence; evaporative coatings for which the substrate presented a large (60°) angle relative to the direction of the evaporation boat provided considerably reduced reflectivity. This is likely to be associated with shadowing effects whereby the islands which are formed early in the coating process cast an effective shadow over adjacent regions, resulting in coating voids and lower overall density. These results are consistent with those from similar studies carried out for the ROSAT mirror coatings (Burkert *et al.* 1986).

4. Sputtered coatings, on the average, outperformed evaporative coatings. This result is expected based upon the higher mobil-

ity provided by the sputtering process, as mentioned above.

5. Iridium coatings provide higher reflectivity than gold coatings, as expected from theoretical calculations.

As a result of these studies, careful consideration of dc-magnetron sputtering and Ir coatings was deemed a significant element of the CPSS.

2 Data Acquisition and Analysis

2.1 SAO Reflectivity Apparatus

The Reflectivity Measurement Apparatus at SAO consists of a long (11.25 m) vacuum pipe equipped with an Imaging Proportional Counter (IPC) (Gorenstein *et al.* 1981) at one end and an x-ray generator at the other. A wide variety of targets and filters are available for generation of x-rays. For this study, measurements were primarily made with a Cu anode followed by a Ni filter. Such a combination provides strong absorption of the Cu-Kβ fluorescence line, as well at the bremsstrahlung component to the spectrum, while transmitting the Cu-Kα line at 8.03 keV (Figure 4). At this energy, the critical angle for iridium falls within the AXAF range of interest (Figure 3). As noted above, reflectivity measurements in the vicinity of the critical angle yield the most sensitive probe for coating anomalies such as reduced density.

The IPC has an intrinsic spatial resolution of approximately 0.25 mm ($\sim$ 0.5 arcmin as viewed from the mirror location) at 8.03 keV. The full field of the IPC is approximately 7.5 cm $\times$ 7.5 cm ($\sim 2^\circ \times 2^\circ$) although, in practice, only the central 3.8 cm in the vertical dimension are utilized. The energy resolution of the IPC is approximately 16% (FWHM) at 8.03 keV, and the limiting data rate is approximately 400 counts s^{-1}. Each photon event is sent through processing electronics and tagged with a position and energy.

As illustrated in Figure 5, x-rays are incident on a test mirror from a distant source and reflected to the IPC; for comparison and simultaneous beam-monitoring, a fixed slit is also imaged in x-rays. The mirror/slit combination is mounted on a motor-driven turntable which may be rotated in order to change the incident grazing angle at the mirror. The turntable is mounted on a translation stage which may be moved to prevent images from falling on the IPC window support ribs. A data acquisition computer is used to collect raw events from the IPC processing electronics as well as to control the positioning of the mirror and slit assembly. In a typical reflectivity run, a scan of approximately 30 angle positions is executed, with finer sampling of the angular dependence in the critical angle area. A typical run requires approximately 3 hours of acquisition time and generates $\sim$ 25 Mbytes of data.

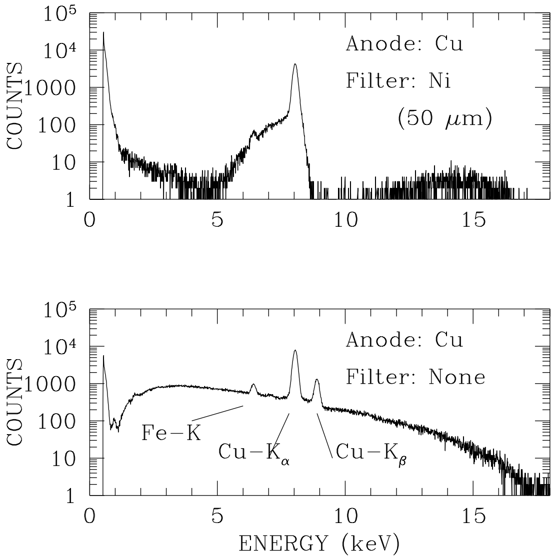

Figure 4: *SSS spectrum of x-ray beam at SAO reflectivity facility, using a copper anode, with an anode voltage of 17 kV. Lower: Unfiltered spectrum in which the Cu-Kα and Cu-Kβ lines are clearly seen superimposed on the bremsstrahlung continuum. Upper: Spectrum after a 50 μm Ni filter is introduced to reduce the continuum and to filter the Cu-Kβ line. Additional lines from Fe, presumably resulting from florescence in the x-ray pipe, are also seen.*

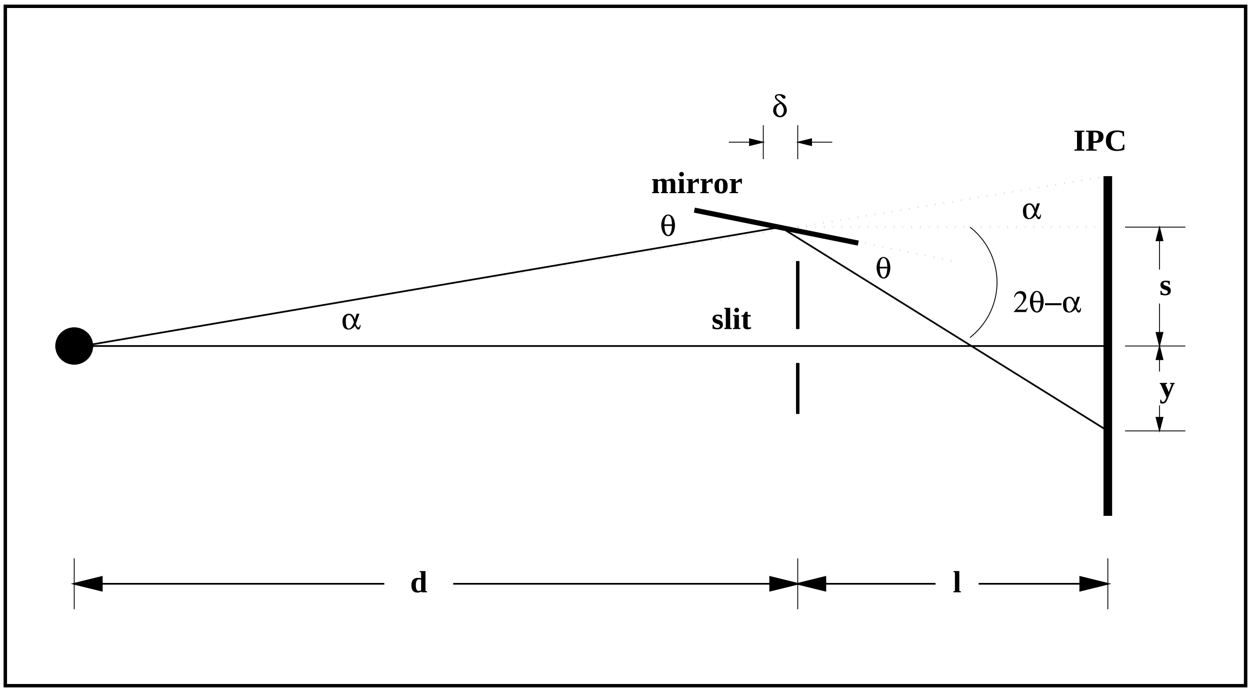

Figure 5: *Schematic illustration of x-ray reflectivity apparatus at SAO.*

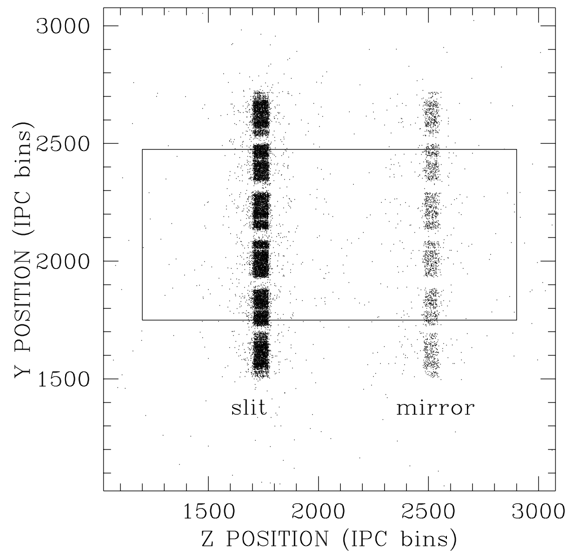

Figure 6: *IPC data showing both slit and mirror images. The rectangular box illustrates manner in which the vertical extent of the images is limited. For each image, events in a 200 bin region centered on the image centroid are used to form the image spectrum.*

2.2 Data Analysis

Analysis of the reflectivity data consists of a three-step procedure:

1. **Event Selection.** The IPC spatial data consists of a 2-d image containing the mirror and slit, as shown in Figure 6. A rectangular subimage is extracted, as indicated in the Figure, to ensure that identical vertical sizes are used for both images. The lateral centroids are then determined for each image, and spectra are extracted from regions extending horizontally ± 100 IPC bins from each centroid, or approximately ± 4.2 arcmin about the specular direction (1 bin $\approx 25\mu$m). Horizontal window support ribs produce regions of x-ray absorption which are identical for the two images, as seen in the Figure.

2. **Angle Determination.** The grazing angle of the mirror is determined analytically, as indicated in Figure 5; the separation of the mirror and slit images is determined by the difference in the relative centroid positions, and all other geometrical factors are measured directly. Using symbols defined in Figure 5, we have
$$\tan(2\theta - \alpha) = \frac{(s+y)}{(l+\delta)} \qquad (12)$$
and
$$\tan\alpha = \frac{s}{d-\delta}. \qquad (13)$$
Thus, the grazing angle θ is given by
$$\theta = \frac{1}{2}\left[\tan^{-1}\left(\frac{s}{d-\delta}\right) + \tan^{-1}\left(\frac{s+y}{l+\delta}\right)\right]. \qquad (14)$$
The values $s = 2.31$ cm, $\delta = 0$, $l = 2.09$ m, and $d = 9.26$ m were fixed for the duration of this study.

3. **Reflectivity Calculation.** The reflectivity for a given mirror of length x is determined by combining the calculated grazing angle with the ratio of counts N_s in the image of a slit of width w with that of the mirror (N_m). Thus,
$$R = \frac{N_m}{N_s}\frac{w}{x\tan\theta}. \qquad (15)$$

The number of counts in each image are extracted from the associated spectrum. A spectral window of 10 PHA bins centered on the centroid of the spectral line is used to provide a roughly monoenergetic measurement (Figure 7). This spectral window is slightly smaller than the FWHM of the spectral response. The line-to-continuum ratio in this band is reasonably high, as verified by measurements carried out with a solid-state spectrometer (Figure 4). In determining the number of counts from the spectral region, endpoint interpolation is carried out to account for noninteger centroid positions.

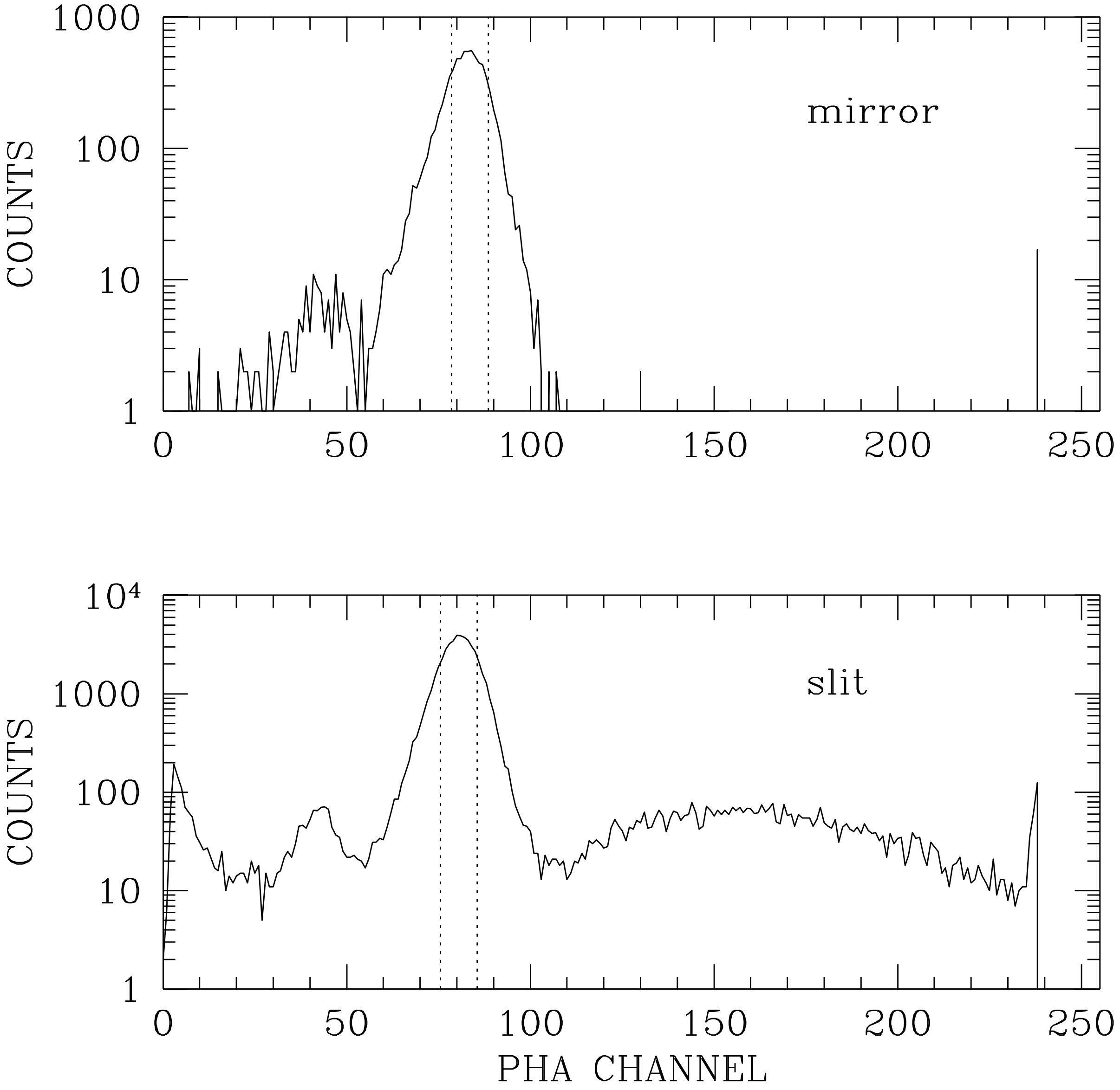

Figure 7: *IPC spectra of slit and mirror for typical reflectivity measurement. The vertical lines represent the spectral window from which events are extracted. Note the lack of high energy x-rays in the x-ray spectrum, due to the decrease in reflectivity with increasing energy.*

Measurement uncertainties are calculated based upon estimated errors in geometrical measurements (which translate into uncertainties in the angle determination, and hence the projection factor which determines the acceptance width of the mirror) and Poisson errors in the number of counts extracted from the spectra. Grazing angle uncertainties are of order 0.2 arcmin or less. Typical relative measurement uncertainties for the reflectivity are approximately 2%. As noted above, a small systematic error in the overall normalization may exist. For comparisons with theoretical reflectivity results, there are additional factors which must also be considered:

1. Because the mirror is illuminated by x-rays over its entire length, the reflectivity is actually averaged over a range of grazing angles. The difference in grazing angle at the two extremes of the mirror is roughly 10% of the nominal grazing angle. At small angles the effect of this deviation is quite small (since the reflectivity changes very slowly with angle in this region); in the critical angle region, however, this variation corresponds to a significant change in reflectivity at the extreme edges of the mirror (though in a partially compensatory way since the reflectivity increases at one end and decreases at the other).

2. The finite spatial window around the image centroid, from which events are selected, results in the inclusion of x-rays which are scattered into a finite angular band around the spectral direction. Because the scattering associated with the surface roughness of the mirror increases with grazing angle, this effect reduces the measured reflectivity at large angles (relative to that measured at small angles). As a result, measured values in close agreement with theory may be obtained at small angles, but not at large angles.

3. While a small correction, the spectral selection does not provide the absolute equivalent of a monoenergetic measurement. Rather, continuum x-rays with energies different from 8.03 keV, but within the spectral resolution of the IPC, will be counted as well. Because the x-ray generator is operated such that the line-to-continuum ratio is very large, this does not represent a large contribution, however.

It must be stressed that these factors, while important, do not enter into the mirror-to-mirror comparisons.

In order to directly compare reflectivity results among different samples, a data-fitting procedure was used to derive the reflectivity at two fiducial angles (20 and 34 arcmin - at which direct measurements were not necessarily made). The procedure (O'Dell 1992) consists of using reflectivity data in the vicinity of the two fiducial angles (data between 10 and 30 arcmin for the 20 arcmin value, and between 30 and 38 arcmin for the 34 arcmin value) to perform a quadratic (20 arcmin) or cubic (34 arcmin) fit to the logarithm of the data. The reflectivity values and associated uncertainties at the fiducial angles are then calculated from the best-fit parameters.

3 Process Selection Study Samples and Reflectivity Results

3.1 Samples

The coated samples used for this study were produced by a variety of techniques. Samples of each type were obtained from at least two different coating manufacturers to provide some level of consistency check on results from a given material and coating process. The substrates for all mirrors were identically prepared, polished zerodur pieces (3" $\times$ 4" $\times$ $\frac{3}{4}$" dimensions). The samples were prepared at MSFC to a flatness specification of $\lambda/2$ (verified by Zygo interferometry at 6328 Å) and a microroughness specification of better than 5 Å RMS in the spatial bandpass 1μm - 500μm (verified by WYKO measurements).

Four different coating materials were investigated: Ir, Au, Pt, and Ni. To eliminate any reflectivity effects associated with coating thickness, the same thickness (350 Å) was used for each coating; a binding layer of Cr (100 Å) was used for each coating to ensure adhesion. Two deposition processes were investigated: e-beam evaporation, and dc-magnetron sputtering. Each coating vendor was required to produce 3 samples coated to identical specifications, but in separate deposition runs. In addition, each vendor provided complete information on the deposition parameters used in producing the coatings, as well as verification that witness samples coated with the mirrors passed a tape-pull adhesion test. A report demonstrating that the deposition procedures used could be scaled to AXAF HRMA size mirrors was also provided. A total of 45 mirrors were procured for the study, as summarized in Table 1.

Table 1: Mirror Inventory for CPSS

Mirror Name	Material	Deposition Technique	Vendor
psaudca1 psaudca2 psaudca3	Gold	dc magnetron sputtering	A
psaudcc1 psaudcc2 psaudcc3	Gold	dc magnetron sputtering	C
psauebb1 psauebb2 psauebb3	Gold	e-beam evaporation	B
psauebd1 psauebd2 psauebd3	Gold	e-beam evaporation	D
psirdca1 psirdca2 psirdca3	Iridium	dc magnetron sputtering	A
psirdcc1 psirdcc2 psirdcc3	Iridium	dc magnetron sputtering	C
psirdcc4 psirdcc5 psirdcc6	Iridium	dc magnetron sputtering	C
psirdce1 psirdce2 psirdce3	Iridium	dc magnetron sputtering	E
psirebb1 psirebb2 psirebb3	Iridium	e-beam evaporation	B
psirebd1 psirebd2 psirebd3	Iridium	e-beam evaporation	D
psptdca1 psptdca2 psptdca3	Platinum	dc magnetron sputtering	A
psptdcc1 psptdcc2 psptdcc3	Platinum	dc magnetron sputtering	C
psptebb1 psptebb2 psptebb3	Platinum	e-beam evaporation	B
psnidca1 psnidca2 psnidca3	Nickel	dc magnetron sputtering	A
psnidce1 psnidce2 psnidce3	Nickel	dc magnetron sputtering	E
psniebb1 psniebb2 psniebb3	Nickel	e-beam evaporation	B

3.2 Results

SAO performed these measurements from March 16 to May 19, 1992. The results of the reflectivity measurements are summarized in Figures 8 - 14 below. In each Figure, data points are compared with a curve representing the theoretical reflectivity from a perfectly smooth, infinitely thick coating with density identical to that of the bulk material. Error bars are shown on one set of data points for each Figure, and are representative of those for the other points (whose errors are not shown, for clarity). Gaps in the angular coverage between 20 and 25 arcmin are the result of the slit image blocking the mirror image.

The data show some indication of a systematic normalization uncertainty, as evidenced by reflectivity values that are too large at the smallest angles. This issue is thought to be associated with uncertainties in the effective width of the slit used in the normalization process, particularly since the effective width is known to exceed the mechanical width due to some x-ray penetration at the slit edges. Mirror-to-mirror comparisons do not suffer from this uncertainty in that the same slit was used for each measurement. This is evident in comparisons of samples produced by the same vendor in different deposition runs, where mirror-to-mirror variations are observed to be negligible for nearly all of the samples. As noted above, a deficiency in measured reflectivity at larger angles may be partially due to x-rays which are scattered at angles larger than the chosen spatial acceptance window.

We discuss the results for each coating material separately:

1. **Gold** The reflectivity results for Au are shown in Figure 8. Little difference is seen between evaporated and sputtered coatings, although it is significant that the mirrors with the lowest reflectivity were produced by evaporation.

2. **Platinum** Results for Pt coatings are shown in Figure 9. Here there is a clear difference between the results from evaporated coatings and coatings produced by sputtering vendor A. Coatings produced by sputtering vendor C, however, performed no better (on average) than the evaporated coatings. This poor performance was attributed to less than optimal choice of sputtering parameters (see discussion regarding Ir samples below). As shown in the Figure, the best Pt results produced reflectivity in excess of the theoretical limit for Au coatings.

3. **Iridium** The results for Ir coatings are plotted in Figure 10. Here there is a dramatic difference between the evaporated and sputtered samples; the evaporated samples produce reflectivities which fall below the theoretical limit for Au - and far below that for Ir - while the best sputtered samples approach theoretical values for Ir. As with the Pt samples, the sputtered samples from vendor C performed poorly in comparison with other sputtered samples. This vendor supplied a 2nd set of mirrors for which the sputter gas pressure and the target-substrate distance were reduced. As discussed in Section 1.1.2, such modifications would be expected to increase the mobility of the depositing atoms, thus increasing the effective density - and, hence, reflectivity - of the resulting coatings. As illustrated in Figure 11, this modification produced the desired results, with the new set of coatings performing as well as the remaining sputtered samples.

4. **Nickel** Reflectivity results for Ni coatings are shown in Figure 12. While interference effects associated with the finite thickness of the coatings make comparisons difficult at larger angles, the results from the different coatings are in excellent agreement at smaller angles and, particularly, through the critical angle region. For this material there seems to be no indication of a preference between the sputtering and evaporation techniques. While the scatter in the interference feature position from vendor to vendor are clearly significant (indicating varying levels of success at obtaining the correct film thickness), sample-to-sample variations from any given vendor are very small, indicating good repeatability.

The reflectivity results for all samples measured in this study are accessible on the CfA HEAD LAN in the directory:

`/home/reflec/ps_results`

The files are in 5 column ASCII format, with the columns containing θ, $d\theta$, R, dR, and the run number. Filenames are of the form `date.mirror.ref` where `date` is the date of measurement and `mirror` is the mirror name. All data may be obtained via anonymous ftp by first sending e-mail to

`slane@cfa.harvard.edu`

requesting that these data be placed in the ftp directory.

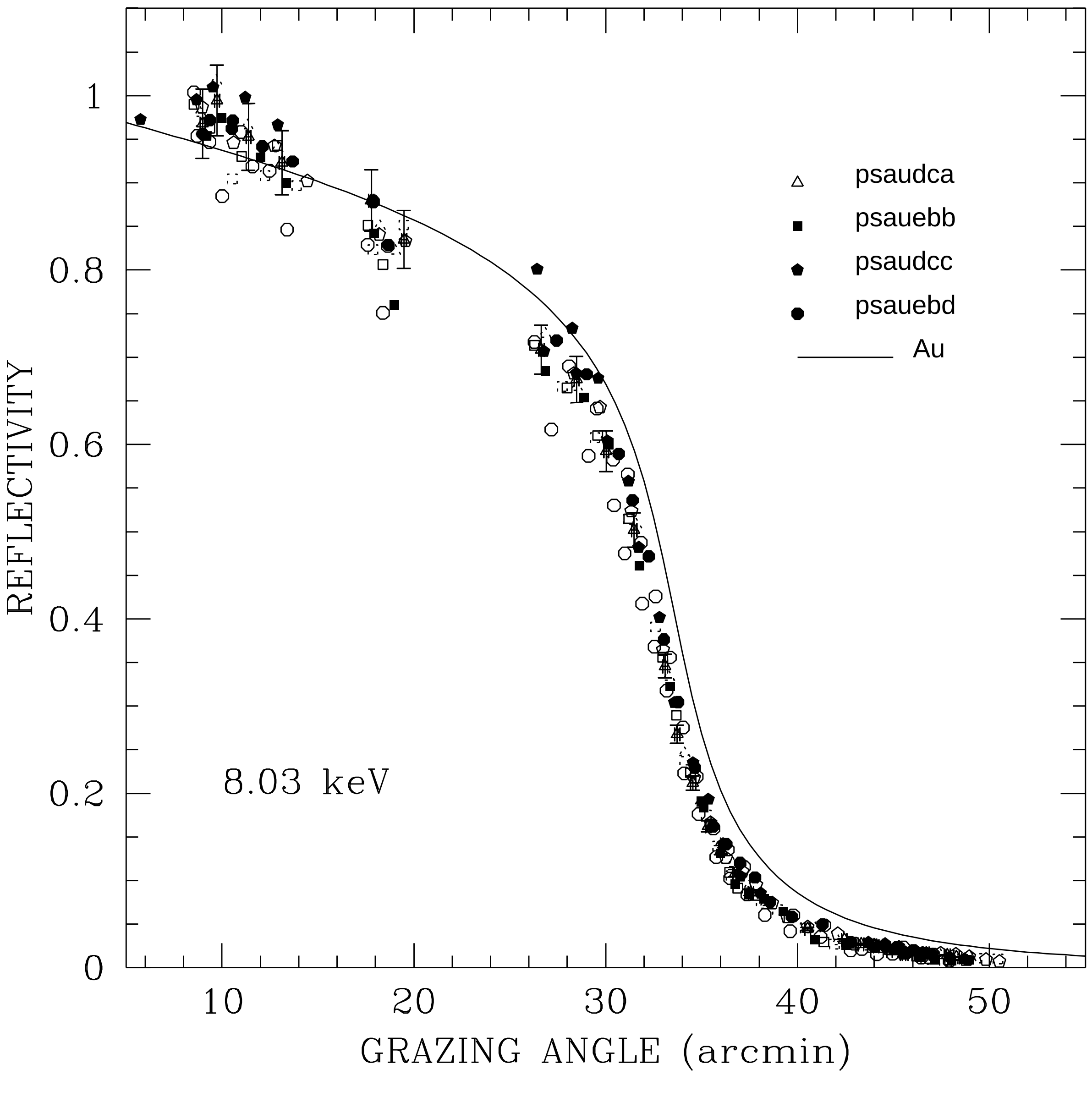

Figure 8: *Comparison of x-ray reflectivity for sputtered and evaporated Au coatings. Solid line corresponds to theoretical reflectivity. Error bars shown on single data set are representative of all data.*

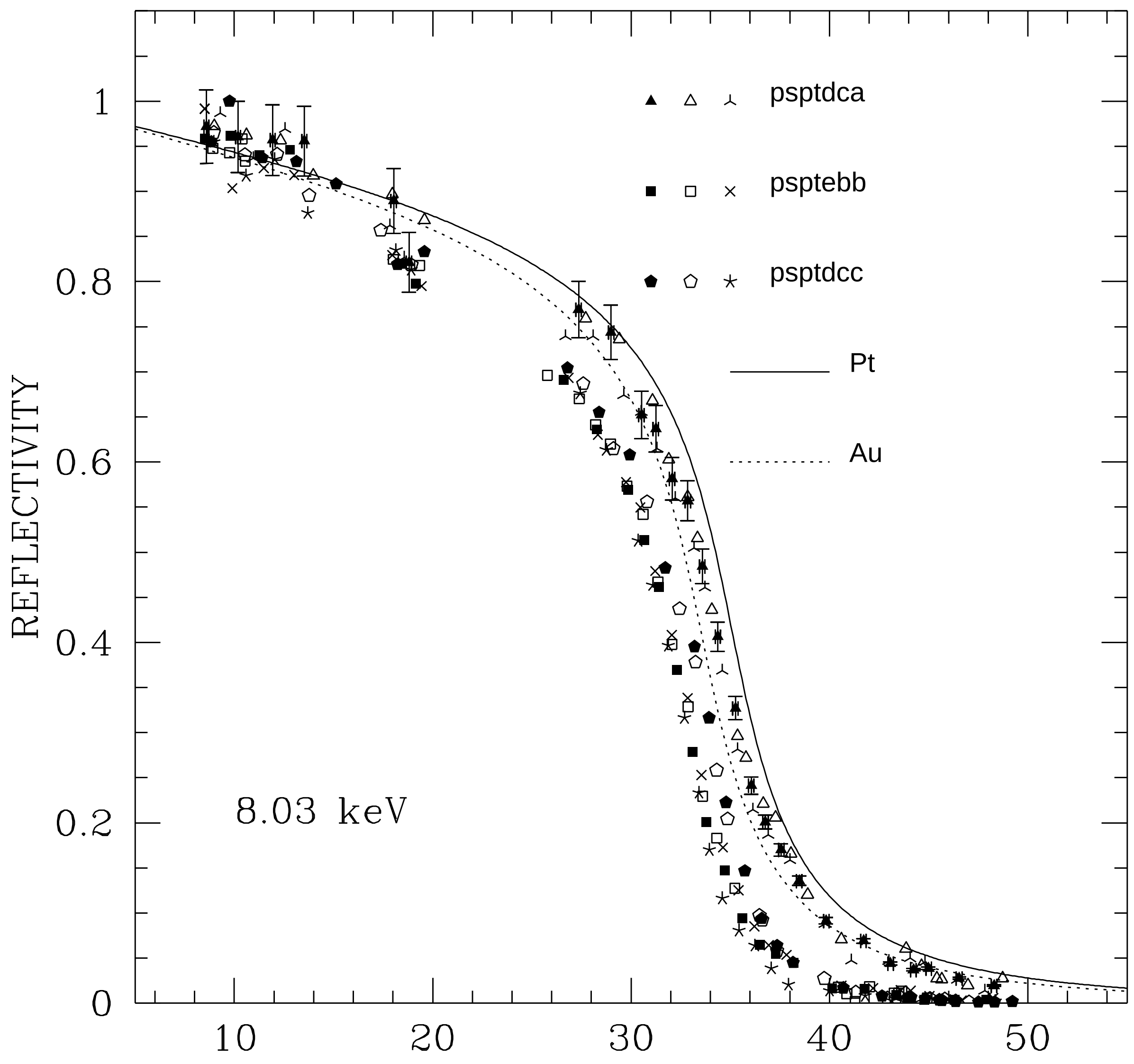

Figure 9: *Comparison of x-ray reflectivity for sputtered and evaporated Pt coatings. Curves correspond to theoretical reflectivity for Pt (solid) and Au (dashed). Error bars shown on single data set are representative of all data.*

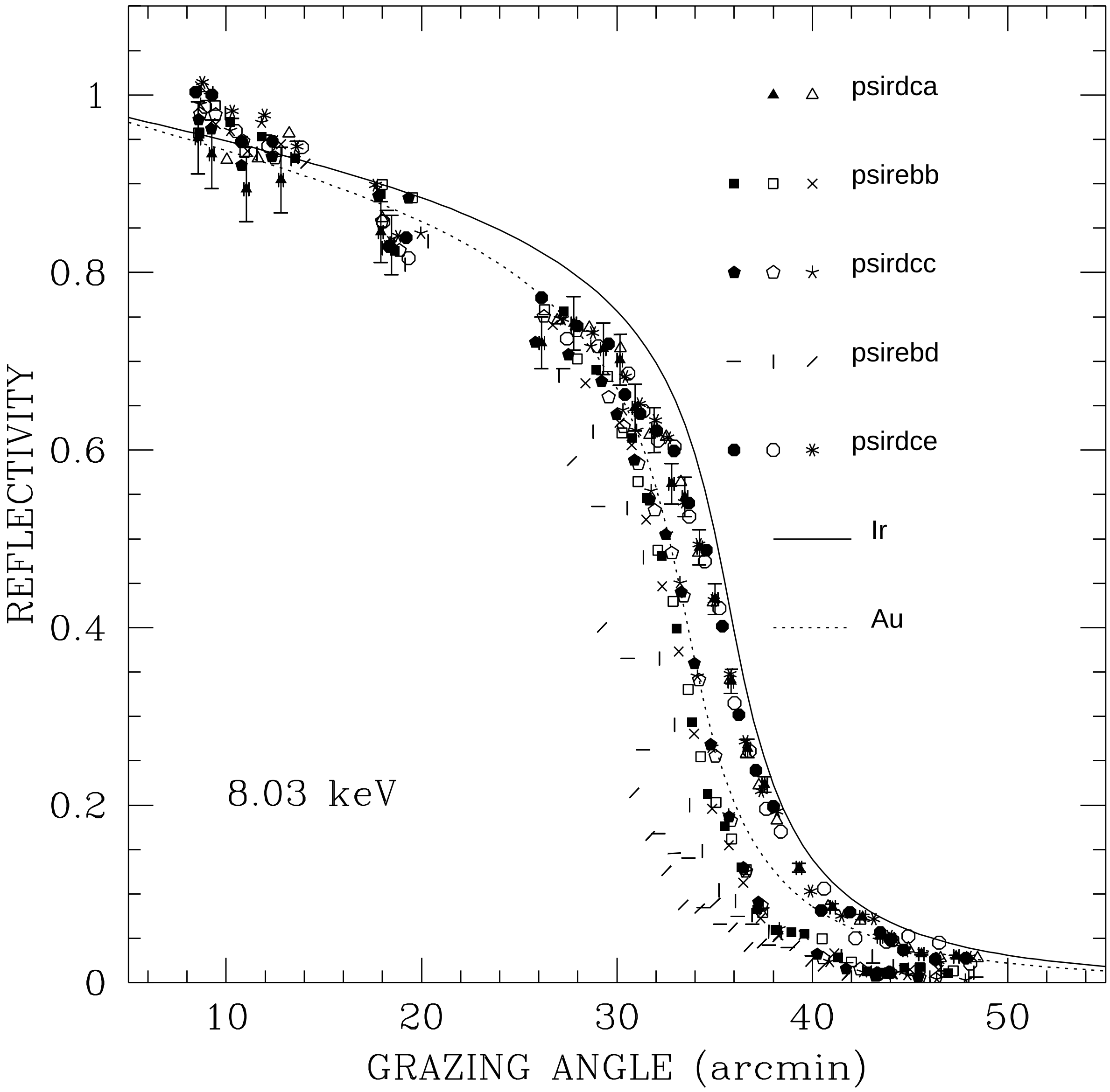

Figure 10: *Comparison of x-ray reflectivity for sputtered and evaporated Ir coatings. Curves correspond to theoretical reflectivity for Ir (solid) and Au (dashed). Error bars shown on single data set are representative of all data.*

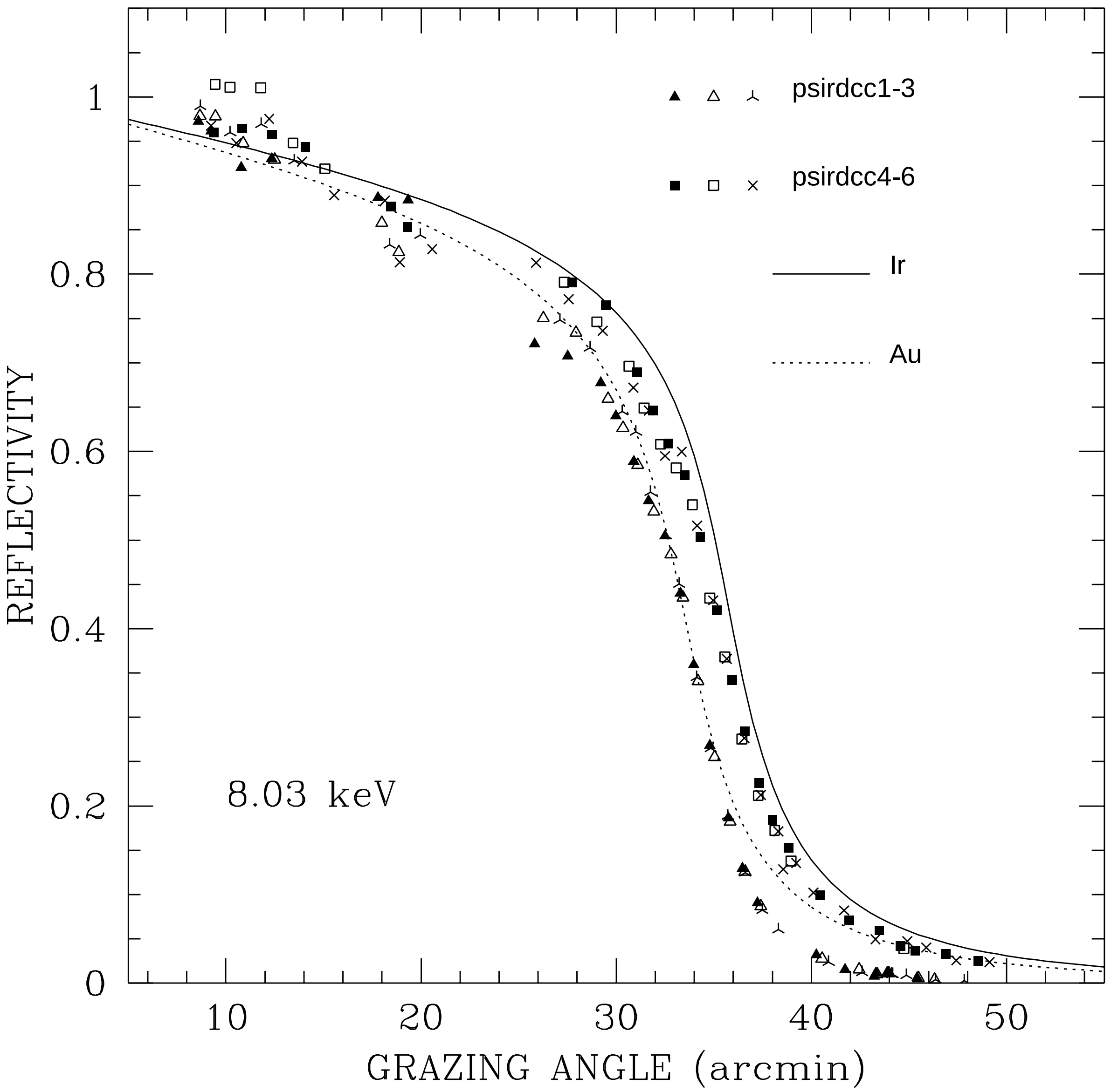

Figure 11: *Comparison of x-ray reflectivity for coatings from vendor C before (triangles) and after (squares) adjustments to sputtering parameters as discussed above.*

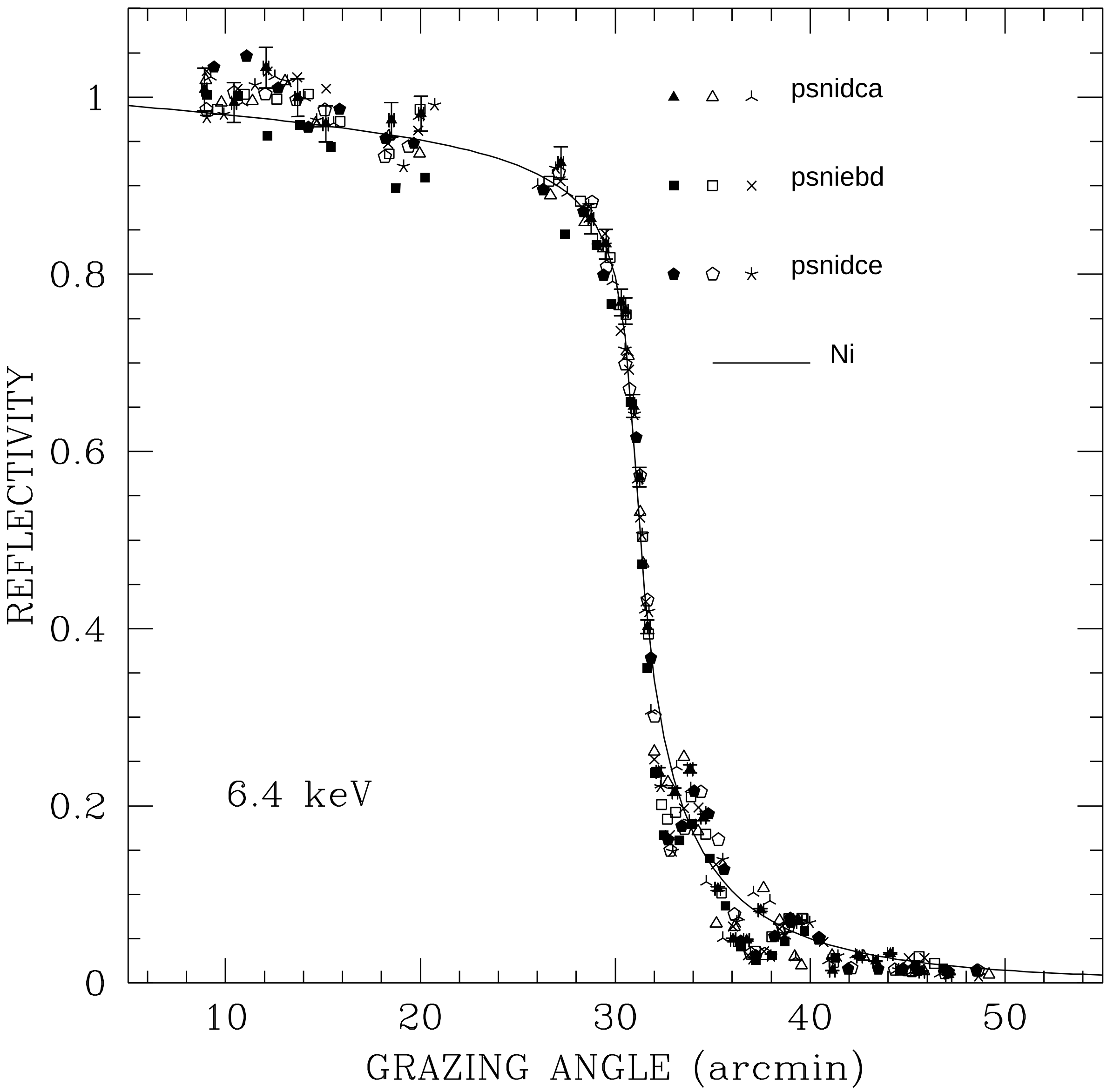

Figure 12: *Comparison of x-ray reflectivity for sputtered and evaporated Ni coatings. Solid line corresponds to theoretical reflectivity. Error bars shown on single data set are representative of all data.*

3.3 Comparisons and Recommendations

An overall comparison of the results summarized above lead to the conclusion that Ir should be the coating material of choice. Figure 13 illustrates a comparison between representative samples of the best Au, Pt, and Ir coatings obtained in the study. It is also clear from the Ir results summarized in Figures 10 and 11 that the deposition method of choice should be a sputtering technique. The results of the study confirm expectations based upon the theoretical reflectivity for each material and the physical principles involved in the deposition processes. In addition, they provide a reflectivity standard upon which the HRMA coating specifications may be based (Section 4.0). The Coating Working Group, based upon the results of this study, has recommended to the AXAF Project that the baseline HRMA coating consist of Ir.

4 Establishment of Coating RFP Specification

Using the Ir reflectivity results summarized above, a minimum specification for the performance of the actual HRMS coating has been derived. The specification is based upon the mean value of the x-ray reflectivity from the sputtered Ir samples (eliminating samples psirdcc1-3 which, as discussed above, were improved upon with modifications to deposition parameters) at two fiducial angles. As described in Section 2.2, the reflectivity at 20 and 34 arcmin was determined for each mirror by performing a fit to the reflectivity values at nearby angles. The results (O'Dell 1992) are summarized in Table 2. The reflectivity specification recommended for the RFP was established as a requirement that the vendor produce a coating which meets or exceeds reflectivity values which are 2σ below the mean, as determined above. This translates into the requirement $\mathrm{R}[20'] \geq 0.81$ and $\mathrm{R}[34'] \geq 0.49$, using the fitting procedure described above.

Table 2: Reflectivities of Sputtered Iridium Samples

Coating	R[20′]	$\sigma_{\mathrm{R}}[20']$	R[34′]	$\sigma_{\mathrm{R}}[34']$
irdca1	0.852	0.009	0.499	0.005
irdca2	0.815	0.008	0.496	0.005
irdcc4	0.842	0.007	0.525	0.005
irdcc5	0.855	0.009	0.508	0.005
irdcc6	0.858	0.008	0.522	0.005
irdce1	0.845	0.009	0.506	0.005
irdce2	0.824	0.008	0.510	0.005
irdce3	0.826	0.008	0.521	0.005
Mean	0.840	0.016	0.511	0.011

5 Vendor Selection Study

In support of the TRW vendor selection process, one additional sample measurement was carried out at SAO. Results from this sputtered Ir sample, supplied by a vendor that had only supplied e-beam evaporation samples for the CPSS, are plotted in Figure 14. It is clear from Figure 14 that the reflectivity from this sample is representative of that from good sputtered Ir mirrors, exceeding the minimum performance specification as indicated by the dashed lines in the Figure.

6 References

Burkert, W. *et al.*, "Effects of Mirror Contamination Observed in the ROSAT Programme", SPIE Proceedings Vol. 733, p. 217-227 (1986)

Elsner, R.F. 1991, "Dielectric and optical constants for AXAF reflecting materials based on data from Henke et al. (1991)," Memorandum W. E. Taylor/EJ31 (August 28, 1991).

Elsner, R.F, O'Dell, S.L., and Weisskopf, M.C. 1991, "Effective Area of the AXAF X-Ray Telescope: Dependence upon Dielectric Constants of Coating Materials," Journal of X-ray Science and Technology, 3, 35-44 (1991)

Gorenstein, P. *et al.* 1981, *Trans. IEEE Nuc. Sci.*, **NS-28**, 869.

Henke, B.L. *et al.* 1982, *Atomic Data and Nuclear Data Tables* **27**(1).

Henke, B.L. *et al.* 1991, to be published.

Loer, S. and Hixson, S. 1991, TRW Interoffice Correspondence - AXAF-91-7-008.

O'Dell, S.L. 1992, Letter to TRW, MSFC, SAO (1992, June 11).

Slane, P.O. 1990a, "AXAF Reflectivity Study Plan", SAO-AXAF-90-031 - Prepared for NASA/MSFC.

Slane, P.O. 1990b, "AXAF X-Ray Reflectivity Studies: Reflectivity of Iridium Coatings", AXAF Interim Report - SAO-AXAF-90-049.

Slane, P.O. *et al.* 1991, "Grazing Incidence X-ray Reflectivity: Studies for the AXAF Observatory", SPIE Proceedings Vol. 1546, p. 26-40 (1991), and AXAF Interim Report - SAO-AXAF-91-016.

Zombeck, M.V. 1983a, "AXAF Effective Area Studies", AXAF Interim Report - SAO-AXAF-83-015.

Zombeck, M.V. 1983b, "Optical Constants and Reflectivities for Nickel, Gold, and Platinum in the X-ray Region of the Spectrum (0.1 - 10 keV)", AXAF Interim Report - SAO-AXAF-83-016.

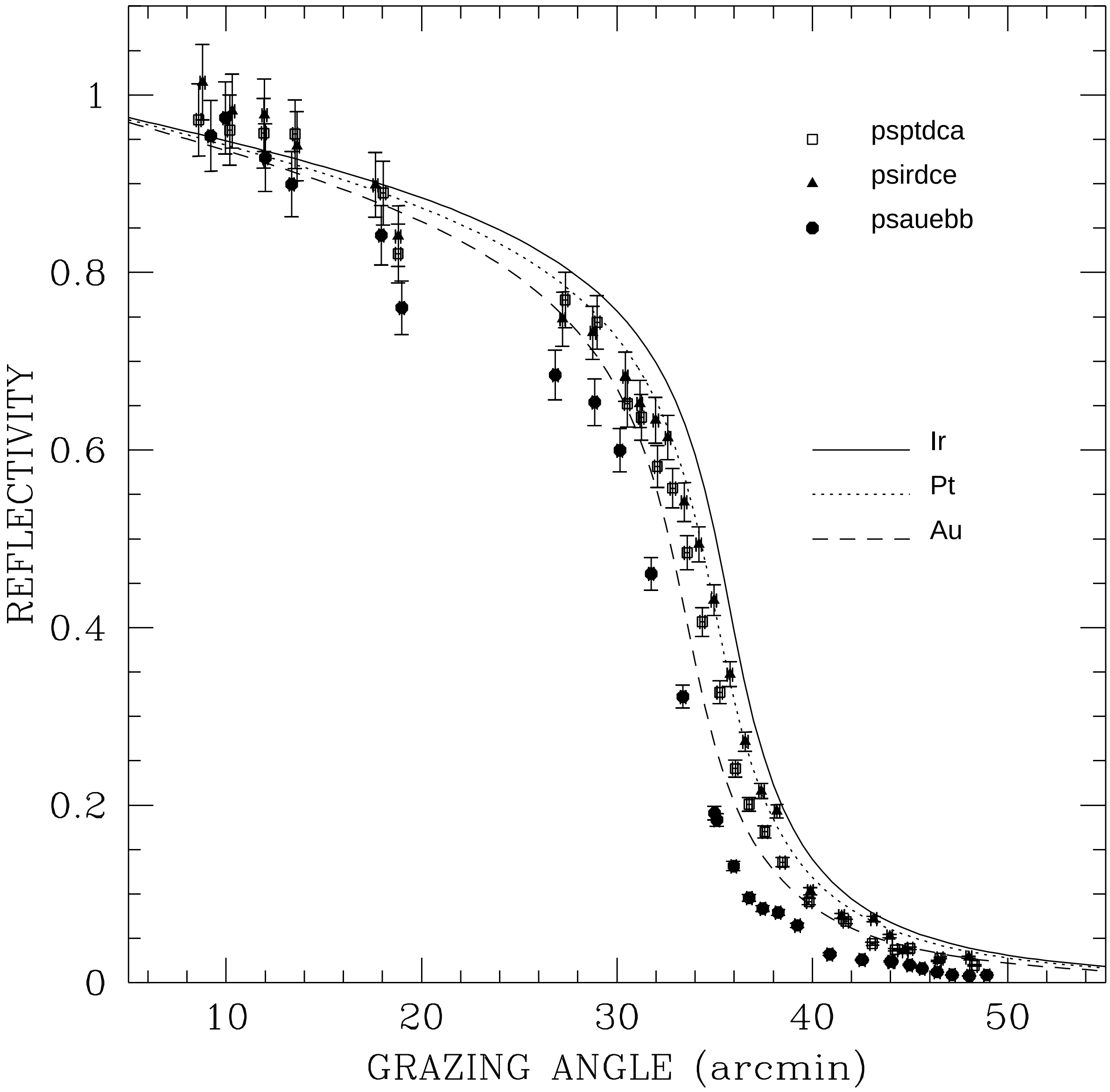

Figure 13: *Comparison between representative samples of the best Au, Pt, and Ir coatings obtained in CPSS. It is clear from these measurements that Ir coatings offer considerably higher reflectivity than the baseline HRMA plan for use of gold.*

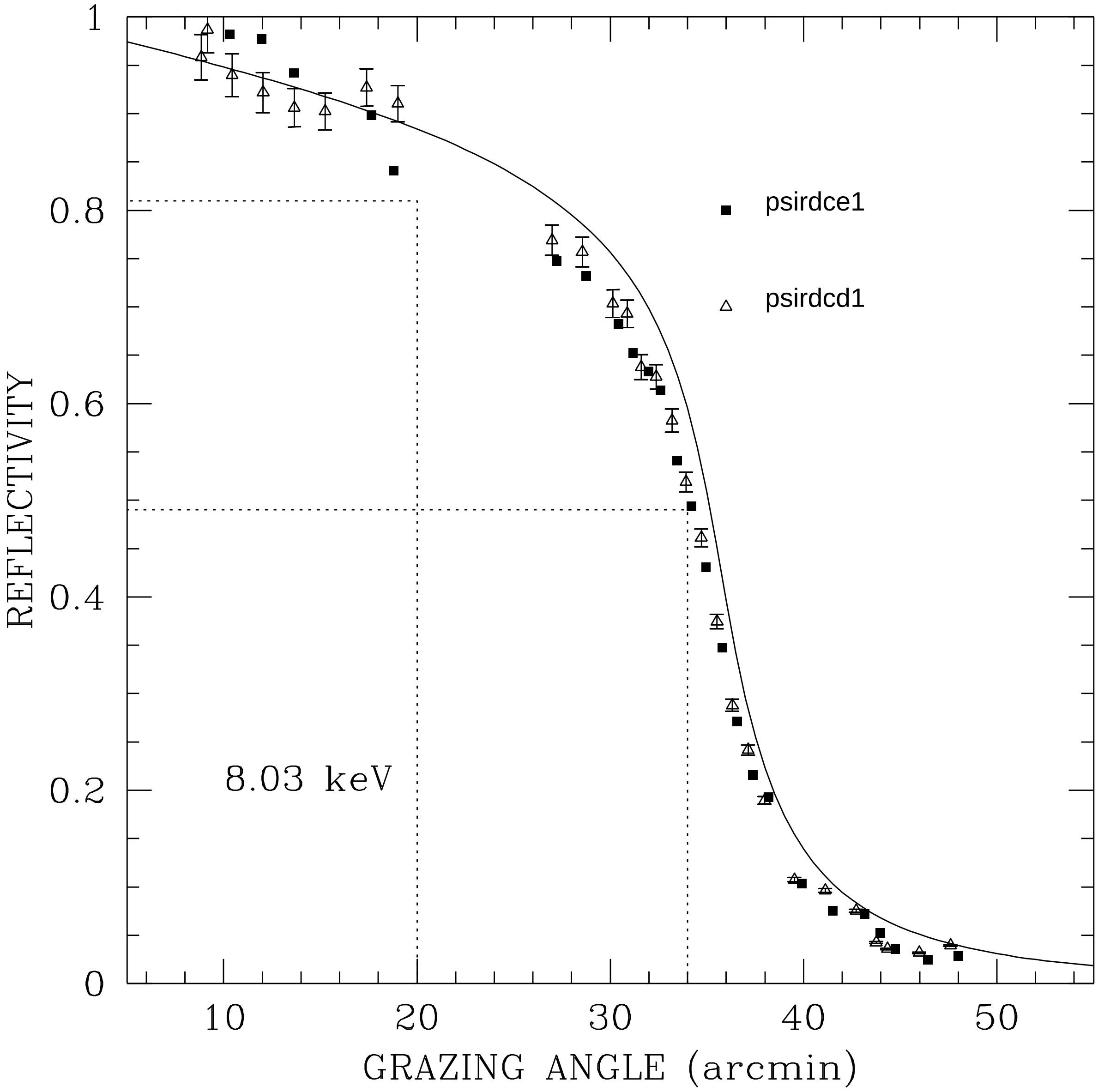

Figure 14: *Comparison of x-ray reflectivity for sample psirdcd1, evaluated in support of vendor proposal evaluation, and psirdce1 which is representative of good sputtered Ir samples. It is clear from the Figure that the new sample performs as well as other sputtered samples. Dashed lines represent minimum performance criterion as described in Section 4.*